



### Science Arts & Métiers (SAM)

is an open access repository that collects the work of Arts et Métiers Institute of Technology researchers and makes it freely available over the web where possible.

This is an author-deposited version published in: <https://sam.ensam.eu>  
Handle ID: <http://hdl.handle.net/10985/8235>

#### To cite this version :

Marc REBILLAT, Rafik HAJRYA, Nazih MECHBAL - Nonlinear structural damage detection based on cascade of Hammerstein models - Mechanical Systems and Signal Processing - Vol. 48, n°1--2, p.247 -- 259 - 2014

Any correspondence concerning this service should be sent to the repository

Administrator : [scienceouverte@ensam.eu](mailto:scienceouverte@ensam.eu)



# Nonlinear structural damage detection based on cascade of Hammerstein models

Marc Rébillat

*PIMM, Arts et Métiers ParisTech, 75013 Paris, France*

Rafik Hajrya

*PIMM, Arts et Métiers ParisTech, 75013 Paris, France*

Nazih Mechbal

*PIMM, Arts et Métiers ParisTech, 75013 Paris, France*

---

## Abstract

Structural damages can result in nonlinear dynamical signatures that can significantly enhance their detection. An original nonlinear damage detection approach is proposed that is based on a cascade of Hammerstein models modelisation of the structure. This model is estimated by means of the Exponential Sine Sweep Method from only one measurement. On the basis of this estimated model, the linear and nonlinear parts of the output are estimated, and two damage indexes (DIs) are proposed. The first DI is built as the ratio of the energy contained in the nonlinear part of an output versus the energy contained in its linear part. The second DI is the angle between the subspaces described by the nonlinear parts of two set of outputs after a principal component analysis. The sensitivity of the proposed DIs to the pres-

---

*Email addresses:* [marc.rebillat@ensam.eu](mailto:marc.rebillat@ensam.eu) (Marc Rébillat),  
[raf.hajrya@gmail.com](mailto:raf.hajrya@gmail.com) (Rafik Hajrya), [nazih.mechbal@ensam.eu](mailto:nazih.mechbal@ensam.eu) (Nazih Mechbal)

ence of damages as well as their robustness to noise are assessed numerically on spring-mass-damper structures and experimentally on actual composite plates with surface-mounted PZT-elements. Results demonstrate the effectiveness of the proposed method to detect nonlinear damage in nonlinear structures and in the presence of noise.

*Keywords:*

Structural health monitoring, non-linear system identification, damage detection.

---

## 1. Introduction

2 The process of implementing a damage detection strategy for aerospace,  
3 civil, and mechanical engineering is referred to as structural health monitor-  
4 ing (SHM). In many cases, damages that appear on complex structures (such  
5 as cracks, impacts, or delaminations) can result in nonlinear dynamical re-  
6 sponses that may be used for damage detection [1–4]. Furthermore, complex  
7 structures often exhibit a nonlinear behavior even in their healthy states. A  
8 robust and reliable SHM system must then be able to deal with nonlinear  
9 damages, and to distinguish between their effects and inherent nonlinearities  
10 in healthy structures. Several limitations of existing methods that are fac-  
11 ing these issues have been recently identified in a report by Farrar *et al.* [1].  
12 The first problem to be addressed is that “*nonlinear behavior does not gen-*  
13 *eralize*”. This implies that the nonlinear models already in use are never  
14 general enough to encompass all the structure encountered in real life. The  
15 second problem is that “*nonlinear approaches are computationally cumber-*  
16 *some, expensive, and requires too many parameters to be defined*”. Currently

17 developed nonlinear models are thus not adequate for practical use of SHM  
18 systems. The work presented here attempts to face these two problems on  
19 the basis of a simple, but rather general, nonlinear model identified by means  
20 of a simple signal processing procedure.

21 In order to build a damage index (DI) that is sensitive to nonlinearities  
22 different approaches have already been proposed [1, 2]. Some DIs are based  
23 on a physical modeling of the damaged structure whereas some are computed  
24 without any physical assumption (black box models). Among these black-box  
25 approaches, some assume a parametric underlying signal processing model,  
26 whereas some are fully non-parametric. To feed these models, random inputs  
27 as well as deterministic broadband or narrowband inputs are used. In this pa-  
28 per, the focus is put on nonlinear damage detection approaches based on DIs  
29 built using a non-parametric black box model estimated using a deterministic  
30 broadband signal. There have been relatively few works in that direction. In  
31 a linear framework, some authors [5, 6] have shown that a nonlinear damage  
32 will impact the transmissibility functions (i.e. the frequency domain ratio  
33 between two different outputs of the system) and they used such information  
34 to detect and locate the damage. Extending the notion of transmissibility  
35 functions to nonlinear systems that can be described by Volterra series, Lang  
36 et. al [7, 8] were able to quantify the decrease of linearity generated by a  
37 nonlinear damage and thus to effectively detect and locate it. However, as  
38 such approaches are focusing on the loss of linearity, they do not seem to be  
39 able to deal with systems that are nonlinear in their healthy states, a fact  
40 that is quite common in real life. To overcome this drawback, several authors  
41 attempted to fit a nonlinear model to the nonlinear structure under study

42 and to compare the actual and predicted outputs, or directly the model co-  
43 efficients, under different damage conditions [9–12]. By doing so, they were  
44 able to detect numerically and experimentally a nonlinear damage even in  
45 an initially nonlinear structure. However, the models they used where para-  
46 metric (mainly frequency domain ARX models) and thus were not easy to  
47 manipulate and neither able to model, without any *a priori* on it, a general  
48 nonlinear structure.

49 We propose here an original approach devoted to nonlinear damage de-  
50 tection in possibly nonlinear structures based on a simple, but rather general,  
51 nonlinear model estimated by means of standard signal processing tools. This  
52 approach is based on the assumption that the structure under study can be  
53 modeled as a cascade of Hammerstein models [13], made of  $N$  branches in  
54 parallel composed of an elevation to the  $n^{\text{th}}$  power followed by a linear fil-  
55 ter called the  $n^{\text{th}}$  order kernel, see Fig. 1(a). The Exponential Sine Sweep  
56 Method [14, 15], previously developed and validated by the authors for dif-  
57 ferent purposes, is then used to estimate the different kernels of the model.  
58 Exponential sine sweeps are a class of sine sweeps that allow estimating a sys-  
59 tem’s  $N$  first kernels in a wide frequency band from only one measurement.  
60 Two damage indexes are then build on the basis of this estimated model.  
61 The first one reflects the ratio of the energy contained in the nonlinear part  
62 of the output versus the energy contained in its linear part and is specially  
63 suited for single-input single-output (SISO) systems. The second one is the  
64 angle between the subspaces described by the nonlinear parts of two set of  
65 outputs after a principal component analysis. This one is specially suited for  
66 single-input multi-output (SIMO) systems. As a first step toward the use

67 of this method for SHM, the sensitivity of the proposed DIs to the presence  
68 of damages as well as their robustness to noise are assessed numerically on  
69 SISO and SIMO systems and experimentally on two actual composite plates  
70 with surface-mounted PZT-elements (one healthy and one damaged).

71 The cascade of Hammerstein models as well as the mathematics behind  
72 it are first described in Sec. 2. The two proposed DIs are then defined in  
73 Sec. 3. Their sensitivity to the presence of damages as well as their robustness  
74 to noise are assessed numerically in Sec 4 and experimentally in Sec. 5. A  
75 general conclusion is finally drawn in Sec. 6.

## 76 **2. Cascade of Hammerstein models estimation using the exponen-** 77 **tial sine sweep method**

### 78 *2.1. Cascade of Hammerstein models*

79 A possible approach to non-linear system identification is to assume that  
80 systems have a given block-structure. Following the “*sandwich*” approach [13],  
81 a non-linear system can be represented as  $N$  parallel branches composed of  
82 three elements in series: a static non-linear part sandwiched between two  
83 linear parts. Such systems are a subclass of Volterra systems and it can be  
84 shown that any continuous non-linear system can be approximated by such  
85 a model [16].

86 Cascade of Hammerstein models are a simplification of this “*sandwich*”  
87 approach. In a cascade of Hammerstein system [13], each branch is composed  
88 of one nonlinear static polynomial element followed by a linear one  $h_n(t)$  as  
89 shown in Fig. 1(a). The relation between the input  $e(t)$  and the output  $s(t)$   
90 of such a system is given by Eq. (1) where “ $(*)$ ” denotes the convolution

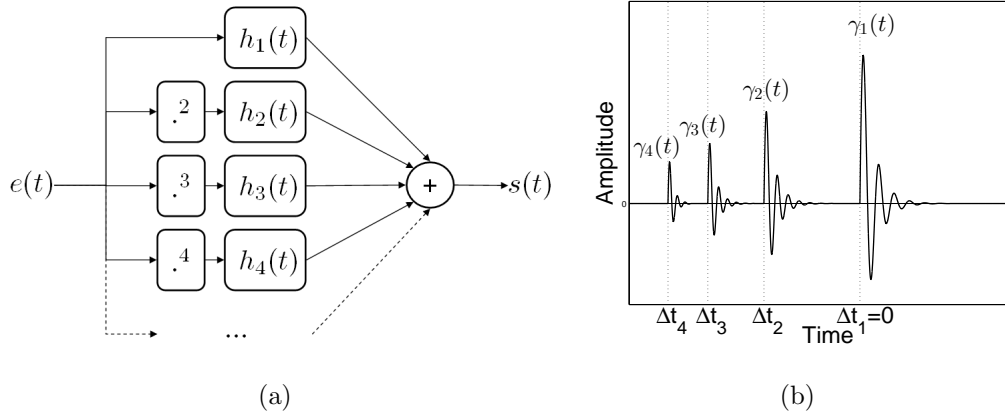


Figure 1: (a) Cascade of Hammerstein model and (b) temporal separation after deconvolution.

91 operator.

$$s(t) = \sum_{n=1}^N (h_n * e^n)(t) \quad (1)$$

92 It can easily be shown from Eq. (1) that cascades of Hammerstein mod-  
 93 els correspond to Volterra models having diagonal Kernels in the temporal  
 94 domain [15]. Thus, cascades of Hammerstein models represent a subclass  
 95 of all the nonlinear “analytical” systems described by Volterra models, and  
 96 are thus rather general nonlinear models. Furthermore, any cascade of Ham-  
 97 merstein models is fully represented by its kernels  $\{h_n(t)\}_{n \in \{1 \dots N\}}$ , which are  
 98 only a set of linear filters. This model is thus also quite simple to use and  
 99 intuitive to understand.

## 100 2.2. Exponential sine sweeps

101 Estimating each kernel  $h_n(t)$  of a cascade of Hammerstein models is not a  
 102 straightforward task. An simple estimation method that has been proposed

103 previously by the authors [15] for this purpose and that is the basis of the  
 104 damage detection procedure is briefly recalled here.

105 To experimentally cover the frequency range over which the system un-  
 106 der study has to be identified, cosines with time-varying frequencies are  
 107 commonly used. Indeed, if  $e(t) = \cos[\phi(t)]$  is the input of the cascade of  
 108 Hammerstein models, the output of the nonlinear block  $e^n(t)$ , see Fig. 1(a),  
 109 can be rewritten using Chebyshev polynomials as in Eq. (2). Details of the  
 110 computation of the Chebyshev matrix  $C = \{c_{n,k}\}$  are provided in [15].

$$\forall n \in [1..N] \quad e^n(t) = \cos^n[\phi(t)] = \sum_{k=0}^n c_{n,k} \cos[k\phi(t)] \quad (2)$$

111 When the instantaneous frequency of  $e(t)$  is increasing exponentially from  
 112  $f_1$  to  $f_2$  in a time interval  $T$ , this signal is called an ‘‘Exponential Sine Sweep’’.  
 113 It can be shown in [14, 15], that by choosing  $T_m = (2m - \frac{1}{2}) \frac{\ln(f_2/f_1)}{2f_1}$  with  
 114  $m \in \mathbb{N}^*$ , one obtains:

$$\forall k \in \mathbb{N}^* \quad \cos[k\phi(t)] = \cos[\phi(t + \Delta t_k)] \quad \text{with} \quad \Delta t_k = \frac{T_m \ln(k)}{\ln(f_2/f_1)} \quad (3)$$

115 Eq. (3) is another expression of the  $k^{\text{th}}$  term in the linearization presented  
 116 in Eq. (2). In summary, for any exponential sine sweep of duration  $T_m$ ,  
 117 multiplying the phase by a factor  $k$  yields to the same signal, advanced in  
 118 time by  $\Delta t_k$ .

### 119 2.3. Kernel recovery in the temporal domain

120 If an exponential sine sweep is presented at the input of a cascade of Ham-  
 121 merstein models, we obtain by combining Eq. (3) and Eq. (1) the following  
 122 relation:



$$s(t) = \sum_{n=1}^N (\gamma_n * e)(t + \Delta t_n) \quad \text{with} \quad \gamma_n(t) = \sum_{k=1}^n C(k, n) h_k(t) \quad (4)$$

123 where  $\gamma_n(t)$  corresponds to the contribution of the different kernels to the  
 124  $n^{\text{th}}$  harmonic.

125 In order to separately identify each kernel  $h_n(t)$  of the cascade of Ham-  
 126 merstein models, a signal  $y(t)$  operating as the inverse of the input signal  
 127  $e(t)$  in the convolution sense, is needed. The Fourier transform  $Y(f)$  of the  
 128 inverse filter  $y(t)$  can be built by means of Eq. (5):

$$Y(f) = \frac{1}{E(f)} \simeq \frac{\overline{E}(f)}{|E(f)|^2 + \epsilon(f)} \quad (5)$$

129 where  $E(f)$  and  $\overline{E}(f)$  are respectively the Fourier transform of  $e(t)$  and its  
 130 complex conjugate, and  $\epsilon(f)$  is a frequency-dependent real parameter chosen  
 131 to be 0 in the bandwidth of interest and to have a large value outside, with  
 132 a continuous transition between the two domains, see [15].

133 After convolving the output of the cascade of Hammerstein models  $s(t)$   
 134 given in Eq. (4) with  $y(t)$ , one obtains Eq. (6), also illustrated in Fig. 1(b):

$$(y * s)(t) = \sum_{n=1}^N \gamma_n(t + \Delta t_n) \quad (6)$$

135 Because  $\Delta t_n \propto \ln(n)$  and  $f_2 > f_1$ , the higher the order of non-linearity  
 136  $n$ , the more advanced is the corresponding  $\gamma_n(t)$ , see Fig. 1(b). Thus, if  $T_m$   
 137 is chosen long enough, the different  $\gamma_n(t)$  do not overlap in time and can be  
 138 separated by simply windowing them in the time domain. Using Eq. (7), the  
 139 family  $\{h_n(t)\}_{n \in [1, N]}$  of the kernels of the cascade of Hammerstein models  
 140 under study can then be fully extracted.

$$\begin{pmatrix} h_1(t) \\ \vdots \\ h_N(t) \end{pmatrix} = \tilde{C}^T \begin{pmatrix} \gamma_1(t) \\ \vdots \\ \gamma_N(t) \end{pmatrix} \quad (7)$$

141 In Eq. (7),  $C^T$  stands for the transpose of the Chebyshev matrix  $C$ , and  
 142  $\tilde{C}$  represents  $C$ , from which the first column and the first row have been  
 143 removed.

144 It can be noticed here that the proposed method is not fully nonpara-  
 145 metric. Indeed, one parameter,  $N$  the order of nonlinearity up to which the  
 146 nonlinear model has to be estimated, is still to be chosen. Its choice mainly  
 147 depends on the noise conditions and on the length of the input exponential  
 148 sine sweep [15].

### 149 **3. Novelty damage indexes**

150 In the case of a structure with distributed actuators and sensors, we can  
 151 consider several configurations to perform damage monitoring. As here an  
 152 active SHM approach has been retained, measurements of one sensor can be  
 153 used by defining a path over the structure that leads to a single-input single-  
 154 output (SISO) system. However, the measurements of all sensors can also be  
 155 used simultaneously, thus defining in that case a single-input multi-output  
 156 (SIMO) system. The two novelty damage indexes proposed in the following  
 157 correspond to these two configurations.

#### 158 *3.1. Decomposition of the output signal into linear and nonlinear parts*

159 By rephrasing Eq. (1) which expresses the output of the cascade of Ham-  
 160 merstein models  $s(t)$  as a function of the input signal  $e(t)$  and of the Ham-

161 merstein kernels  $\{h_n(t)\}_{n \in [1, N]}$ , it is possible to decompose the output of the  
 162 cascade of Hammerstein models as follows:

$$s(t) = (h_1 * e)(t) + \sum_{n=2}^N (h_n * e^n)(t) = s^L(t) + s^{\text{NL}}(t) \quad (8)$$

163 where  $s^L(t) = (h_1 * e)(t)$  stand for the linear and  $s^{\text{NL}}(t) = \sum_{n=2}^N (h_n * e^n)(t)$   
 164 the nonlinear parts of the output signal  $s(t)$ .

165 As the input signal  $e(t)$  is known and as the Hammerstein kernels  $\{h_n(t)\}_{n \in [1, N]}$   
 166 have been estimated previously, those linear and nonlinear parts of the output  
 167 signal are then easily evaluated and can be used to build damage indexes.

### 168 3.2. $DI_1$ : Ratio of the nonlinear energy to the linear energy

169 In the single-input, single-output case (SISO), there is only one input  
 170  $e(t)$  and one output  $s(t)$ . Taking advantage of Eq. (8), we propose a damage  
 171 index (DI) that is defined as the ratio of the energy contained in the nonlinear  
 172 part of the output of the cascade of Hammerstein models versus the energy  
 173 contained in the linear part of the output of the cascade of Hammerstein  
 174 models. By denoting  $S^L(f)$  and  $S^{\text{NL}}(f)$  the Fourier transform of  $s^L(t)$  and  
 175  $s^{\text{NL}}(t)$ , we propose a damage index defined as follow:

$$DI_1 = \frac{\int_{f_1}^{f_2} |S^{\text{NL}}(f)|^2 df}{\int_{f_1}^{f_2} |S^L(f)|^2 df} \quad (9)$$

176 where  $f_1$  and  $f_2$  have been defined earlier in Sec. 2.2.

177 In a given composite structure, as the nonlinear damage (impact, delami-  
 178 nation, or crack) becomes more severe, it is expected to contribute more and  
 179 more to the nonlinear part of the output  $s^{\text{NL}}(t)$ . As a consequence,  $DI_1$  is

180 expected to be sensitive to the presence of the damage, but also to its ex-  
 181 tent. This will be demonstrated numerically in Sec. 4.3 and experimentally  
 182 in Sec. 5.

### 183 3.3. $DI_2$ : Angle between nonlinear subspaces

184 In the single-input, multiple-output framework (SIMO), there is still one  
 185 input  $e(t)$  but now  $J$  outputs  $\{s_j(t)\}_{j \in [1..J]}$ . Taking advantage of Eq. (8),  
 186 it is still possible to decompose each output  $s_j(t)$  into its linear  $s_j^L(t)$  and  
 187 nonlinear  $s_j^{\text{NL}}(t)$  parts. Following previous work by the authors [17], the idea  
 188 is then to monitor the subspaces spanned by the nonlinear parts of each  
 189 outputs set.

190 In a discrete-time matrix form, let  $\mathbf{s}^{\text{NL}} \in \mathbb{R}^{U \times J}$  be the nonlinear parts of  
 191 the  $J$  output signals having each a length of  $U$  samples. Let  $\mathbf{A}^{\text{NL}} \in \mathbb{R}^{U \times J}$   
 192 be the separating matrix of  $\mathbf{s}^{\text{NL}}$ . This matrix is obtained from a principal  
 193 component analysis technique [18] and is defined as follows:

$$\mathbf{A}^{\text{NL}} = \mathbf{\Lambda}_{\mathbf{s}^{\text{NL}}}^{-\frac{1}{2}} \times (\mathbf{P}^{\text{NL}})^{\text{T}} \quad (10)$$

194 where  $\mathbf{P}^{\text{NL}} = [\underline{\mathbf{p}}_1^{\text{NL}}, \dots, \underline{\mathbf{p}}_J^{\text{NL}}]$  is the matrix of eigenvectors of  $\mathbf{s}^{\text{NL}}$  and  
 195  $\mathbf{\Lambda}_{\mathbf{s}^{\text{NL}}}$  is the diagonal matrix of eigenvalues of  $\mathbf{s}^{\text{NL}}$ . If the reduction using  
 196 singular value decomposition (SVD) is possible [19], the separating matrix  
 197 can then be rewritten as follows:

$$\begin{aligned}
\mathbf{A}^{\text{NL}} &= \mathbf{I}_{J \times J} \times \mathbf{\Gamma}^{\text{NL}} \times (\mathbf{V}^{\text{NL}})^{\text{T}} \tag{11} \\
&= \begin{bmatrix} \mathbf{I}_{J \times J_p} & \mathbf{I}_{J \times (J-J_p)} \end{bmatrix} \begin{bmatrix} \mathbf{\Gamma}_1^{\text{NL}} & \mathbf{0} \\ \mathbf{0} & \mathbf{\Gamma}_2^{\text{NL}} \end{bmatrix} \begin{bmatrix} \mathbf{V}_1^{\text{NL}} & \mathbf{V}_2^{\text{NL}} \end{bmatrix}^{\text{T}} \\
&= \mathbf{A}_1^{\text{NL}} + \mathbf{A}_2^{\text{NL}}
\end{aligned}$$

198 where  $\mathbf{\Gamma}_1^{\text{NL}} = \text{diag}(\sigma_1, \dots, \sigma_{J_p})$ ,  $\mathbf{V}_1^{\text{NL}} = [\mathbf{v}_{1_1}^{\text{NL}}, \dots, \mathbf{v}_{1_{J_p}}^{\text{NL}}] \in \mathbb{R}^{U \times J_p}$  and  
199  $\mathbf{A}_1^{\text{NL}} \in \mathbb{R}^{U \times J_p}$  are respectively the matrix of singular values, the matrix of  
200 right singular vectors, and the separating matrix associated to the princi-  
201 pal subspace of  $\mathbf{s}^{\text{NL}}$ .  $\mathbf{\Gamma}_2^{\text{NL}} = \text{diag}(\sigma_{J_p+1}, \dots, \sigma_J)$ ,  $\mathbf{V}_2^{\text{NL}} = [\mathbf{v}_{1_{J_p+1}}^{\text{NL}}, \dots, \mathbf{v}_{1_J}^{\text{NL}}] \in$   
202  $\mathbb{R}^{U \times (J-J_p)}$  and  $\mathbf{A}_2^{\text{NL}} \in \mathbb{R}^{U \times (J-J_p)}$  are respectively the matrix of singular val-  
203 ues, the matrix of right singular vectors, and the separating matrix associated  
204 to the residual subspace of  $\mathbf{s}^{\text{NL}}$ .

205 Let  $\mathbf{A}_1^{\text{NL}}$  and  $\tilde{\mathbf{A}}_1^{\text{NL}}$  be two matrices built as described previously from  
206 measurements in a healthy state and in an unknown state. Let's  $R\{(\mathbf{A}_1^{\text{NL}})^{\text{T}}\}$   
207 and  $R\{(\tilde{\mathbf{A}}_1^{\text{NL}})^{\text{T}}\}$  be the range subspaces of matrices  $(\mathbf{A}_1^{\text{NL}})^{\text{T}}$  and  $(\tilde{\mathbf{A}}_1^{\text{NL}})^{\text{T}}$ ,  
208 and  $\mathbf{P}_{R\{(\mathbf{A}_1^{\text{NL}})^{\text{T}}\}}$  and  $\mathbf{P}_{R\{(\tilde{\mathbf{A}}_1^{\text{NL}})^{\text{T}}\}}$  the orthogonal projections on these range  
209 subspaces obtained though SVD (see [17] for details). We then denote  
210  $\underline{\phi} \left[ R\{(\mathbf{A}_1^{\text{NL}})^{\text{T}}\}, R\{(\tilde{\mathbf{A}}_1^{\text{NL}})^{\text{T}}\} \right]$  the principal angle vectors between the range  
211 subspaces  $R\{(\mathbf{A}_1^{\text{NL}})^{\text{T}}\}$  and  $R\{(\tilde{\mathbf{A}}_1^{\text{NL}})^{\text{T}}\}$ . Using the SVD tool, the Euclidean  
212 norm of the sinus of this angle is defined as follow [20]:

$$\begin{aligned}
\| \sin \left( \underline{\phi} \left[ R\{(\mathbf{A}_1^{\text{NL}})^{\text{T}}\}, R\{(\tilde{\mathbf{A}}_1^{\text{NL}})^{\text{T}}\} \right] \right) \|_2 &= \| \mathbf{P}_{R\{(\mathbf{A}_1^{\text{NL}})^{\text{T}}\}^\perp} \times \mathbf{P}_{R\{(\tilde{\mathbf{A}}_1^{\text{NL}})^{\text{T}}\}} \|_2 \tag{12} \\
&= \| (\mathbf{I}_{J_p \times J_p} - \mathbf{P}_{R\{(\mathbf{A}_1^{\text{NL}})^{\text{T}}\}}) \times \mathbf{P}_{R\{(\tilde{\mathbf{A}}_1^{\text{NL}})^{\text{T}}\}} \|_2
\end{aligned}$$

213 We then propose to define a damage index as:

$$\text{DI}_2 = \frac{\left\| \sin \left( \underline{\phi} \left[ R\{(\mathbf{A}_1^{\text{NL}})^{\text{T}}\}, R\{(\tilde{\mathbf{A}}_1^{\text{NL}})^{\text{T}}\} \right] \right) \right\|_2}{J_p} \quad (13)$$

214 where  $J_p$  is the number of principal components retained in the principal  
 215 subspaces. This damage index can be interpreted as the angle between the  
 216 subspaces described by the nonlinear parts of the outputs in the healthy state  
 217 and in the unknown state.

218 In a given composite structure, as the nonlinear damage becomes more  
 219 severe, it is expected to contribute more and more to the nonlinear parts of  
 220 the different outputs  $\{s_j(t)\}_{j \in [1..J]}$  and then to increase the angle between  
 221 the associated principal subspaces. As a consequence,  $\text{DI}_2$  is expected to be  
 222 sensitive to the presence of the damage, but also to its extent. This will be  
 223 demonstrated numerically in Sec. 4.4 and experimentally in Sec. 5.

## 224 4. Simulation results

### 225 4.1. Simulated systems

226 In order to validate the proposed approach and the associated novelty  
 227 damage indexes, numerical simulations have been carried out for single-input,  
 228 single-output (SISO) and single-input, multi-output (SIMO) systems. The  
 229 systems that have been chosen are simple one degree of freedom and five  
 230 degrees of freedom spring-mass-damper (SMD) systems and are shown in  
 231 Fig. 2.

232 The damage in those systems has been introduced by means of a bilinear  
 233 stiffness  $k[x(t)]$  as a very easy way to simulate a breathing crack. Such cracks

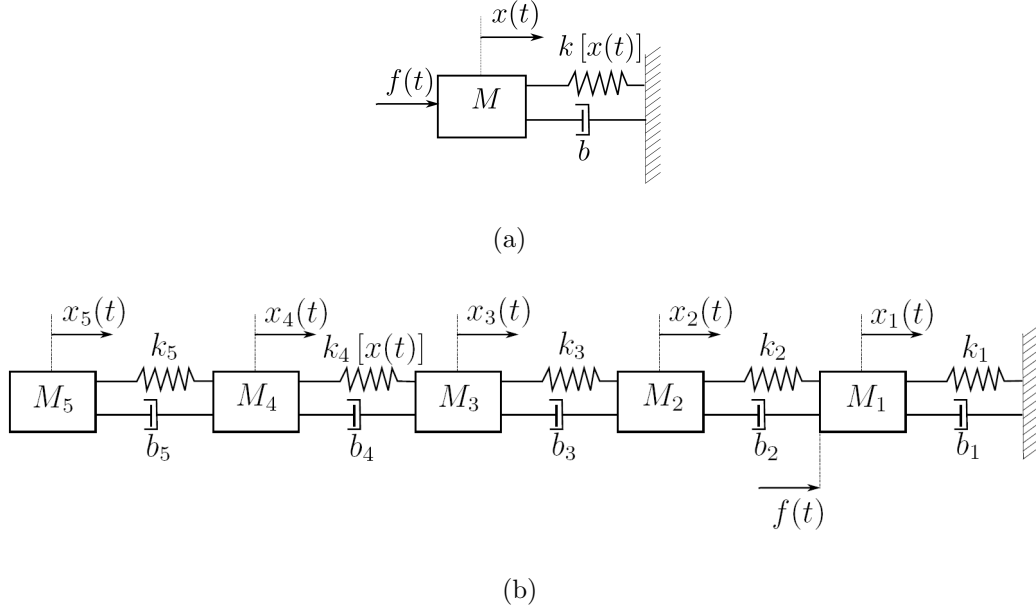


Figure 2: (a) Simulated single degree of freedom SISO system and (b) simulated five degrees of freedom SIMO system.

234 have a lower stiffness when the crack is open than when the crack is closed.  
 235 Thus, the bilinear stiffness is defined as follows:

$$k[x(t)] = \begin{cases} k^I & \text{if } x(t) < 0 \\ (1 - \alpha)k^I & \text{if } x(t) > 0 \end{cases} \quad (14)$$

236 In this definition,  $k^I$  denotes the linear stiffness of the original undamaged  
 237 system and the *damage-parameter* is the coefficient  $\alpha$ . If  $\alpha = 0$ , the stiffness  
 238 is fully linear and the system is healthy. If  $\alpha = 1$ , the stiffness when the  
 239 crack is open is null and thus, the system is fully damaged.

240 The chosen SISO system is a SMD system where the input is the force  
 241  $f(t)$  applied to the mass  $M$  and the output is the displacement  $x(t)$  of the  
 242 mass  $M$ , as shown in Fig. 2(a). For this system  $M = 1$  kg,  $b = 2$  Ns/m and

243  $k^I = 20000$  N/m.

244 The chosen SIMO system is a serie of five SMD systems where the input is  
245 the force  $f(t)$  applied to the mass  $M_1$  and the outputs are the displacements  
246  $\{x_1(t), \dots, x_5(t)\}$  of the masses  $\{M_1, \dots, M_5\}$  as shown in Fig. 2(b). The  
247 damage is introduced by means of the bilinear stiffness  $k_4[x(t)]$  as defined by  
248 Eq. (14). For this system  $M_1 = M_2 = M_3 = M_4 = M_5 = 1$  kg,  $b_1 = b_2 = b_3 =$   
249  $b_4 = b_5 = 2$  Ns/m,  $k_1 = k_2 = k_3 = k_5 = 20000$  N/m, and  $k_4^I = 20000$  N/m.

#### 250 4.2. Input signal

251 In order to estimate the linear and nonlinear parts in the ouput of this  
252 system, an input signal has been designed as described in Sec. 2.2. The start  
253 and stop frequencies have been chosen as  $f_1 = 2.25$  Hz and  $f_2 = 225$  Hz,  
254 knowing that  $f_r = 25$  Hz is the resonance frequency of both undamaged  
255 systems. The sweep duration has been chosen as  $T = 8.86$  seconds for the  
256 SISO system and  $T = 88.6$  seconds for the SIMO system both with an input  
257 amplitude of  $E = 0.1$  N. The response of this system to this input signal has  
258 been simulated using *Simulink*<sup>TM</sup> with a fixed-step Runge-Kutta algorithm  
259 running at  $f_s = 563$  Hz. A zero-mean Gaussian white noise has been added  
260 to the input of the simulation in order to simulate environmental noise. It is  
261 assumed that environmental noise is larger than measurement noise, and thus  
262 no noise has been added to the output of the simulation. To illustrate the  
263 robustness of the proposed DIs to noise, the noise variance has been chosen  
264 as a function of the root-mean-square power of the input signal in order to  
265 have a signal to noise ratio (SNR) of 60 or 30 dB (i.e. a noise with a standard  
266 deviation of  $6 \times 10^{-5}$  N or  $2 \times 10^{-3}$  N). Simulation have been carried out  
267 for values of  $\alpha$  ranging from 0 (healthy state) to 0.45 (half-damaged state)



268 by steps of 0.025. For each  $\alpha$  value, the simulations have been repeated 30  
 269 times in order to compute the mean and standard deviation of both DIs when  
 270 subjected to noise.

271 *4.3. Damage detection using  $DI_1$  for the SISO system*

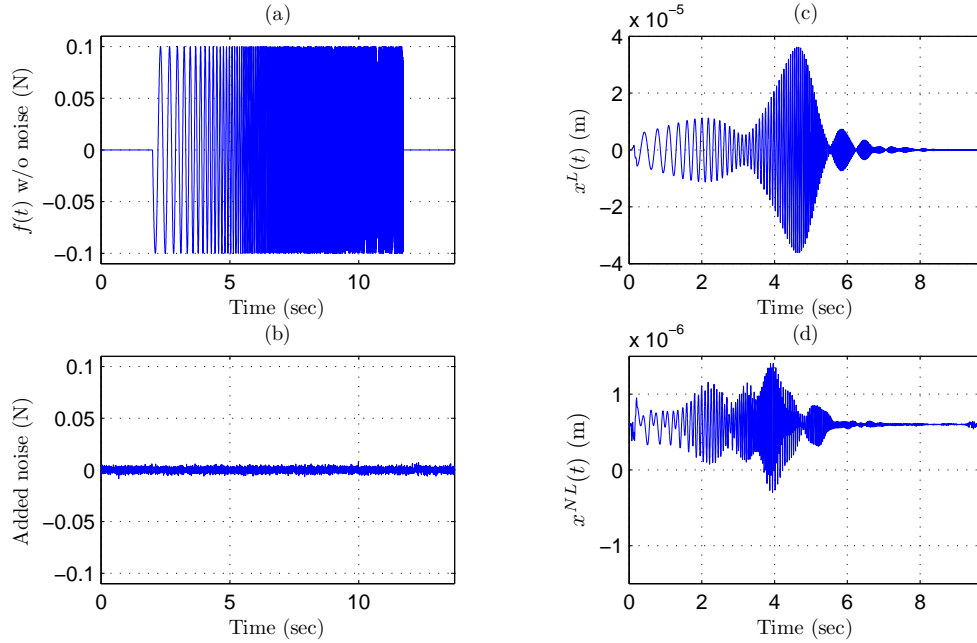


Figure 3: (a) Input sweep without noise and (b) added noise for a SNR of 30 dB. Estimated (c) linear and (d) nonlinear parts of the output signal  $x(t)$ .

272 The noise-free input signal, the added noise, and the estimated linear  
 273  $x^L(t)$  and nonlinear  $x^{NL}(t)$  parts of the output signal  $x(t)$  of the system of  
 274 Fig. 2(a) are shown on Fig. 3. From this figure, it can be seen that a SNR of  
 275 30 dB implies the addition of a relatively large amount of noise to the input  
 276 signal. Furthermore, by analyzing the estimated linear part of the output

277 signal  $x^L(t)$ , it can be seen that, as expected, the chosen nonlinear system  
 278 basically acts as a resonant filter. Finally, it can be seen that the system  
 279 under study is effectively nonlinear as a non-null nonlinear part  $x^{NL}(t)$  in  
 280 the output signal is being estimated by the previously described procedure.

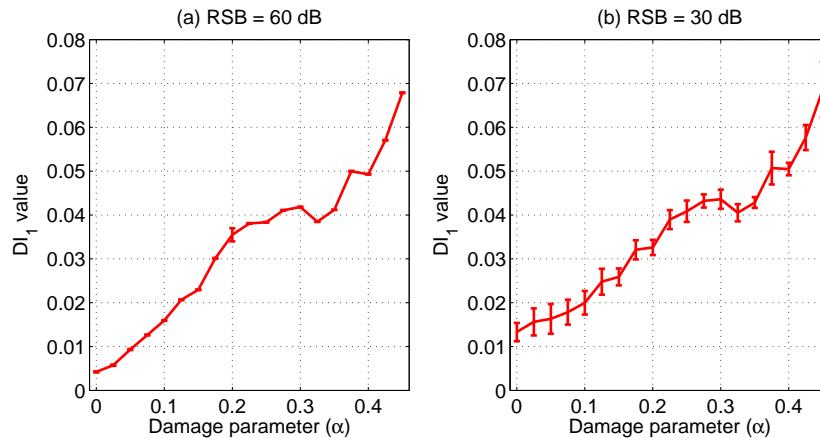


Figure 4: Average and standard deviation of the  $DI_1$  values for different values of the damage parameter  $\alpha$  with (a) SNR= 60 dB and (b) SNR= 30 dB.

281 In Fig. 4 the averages and standard deviations over the 30 trials of the  
 282  $DI_1$  values for the different values of the damage parameter  $\alpha$  and with  
 283 SNR= 60 dB and SNR= 30 dB are shown. First of all, it can be seen  
 284 that the damage index  $DI_1$  increases in both cases almost monotonically with  
 285 the damage parameter  $\alpha$ . Moreover, even when the noise power is relatively  
 286 large (see the curve for SNR= 30 dB) the standard deviations remain small  
 287 around the average values. Finally, for a value of the damage parameter  
 288  $\alpha = 0$  (*i.e.* in the linear case), the  $DI_1$  value should be zero and is found dif-  
 289 ferent from zero. This thus means that a part of the noise is here interpreted  
 290 by the estimation process as a nonlinear part of the output. We can thus

291 conclude from that simulation that the damage index  $DI_1$  is able to detect  
 292 and to quantify the amount of damage in the nonlinear system with a high  
 293 robustness to noise.

294 *4.4. Damage detection using  $DI_2$  for the SIMO system*

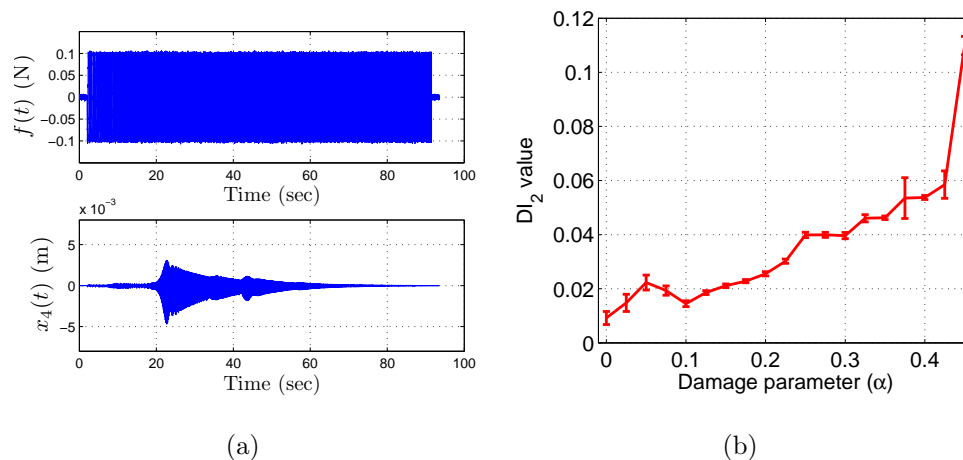


Figure 5: (a) Input signal  $f(t)$  (top) and output signal  $x_4(t)$  for  $\alpha = 0.45$  (bottom).  
 (b) Average and standard deviation of the  $DI_2$  values for different values of the damage parameter  $\alpha$  and for a SNR of 30 dB.

295 In Fig. 5(a) the noisy input signal  $f(t)$  as well as one of the five output  
 296 signals,  $x_4(t)$ , of the system of Fig. 2(b) are shown. It can be seen that  
 297 as previously the nonlinear system of Fig. 2(b) filters the input signal and  
 298 possesses a clear resonant frequency in the bandwidth under study. Further-  
 299 more, the fact that this system is nonlinear can be easily seen as the output  
 300 signal is not symmetrical with respect to the horizontal axis. In Fig. 5(b)  
 301 the averages and standard deviations over the 30 trials of the  $DI_2$  values  
 302 computed by retaining  $J_p = 5$  principal components for the different values

303 of the damage parameter  $\alpha$  and for a SNR of 30 dB are shown. First of all,  
304 it can be seen that again the damage index  $DI_2$  increases almost monotonically  
305 with the damage parameter  $\alpha$ . Moreover, even if the noise power is relatively  
306 large (SNR= 30 dB) the standard deviations still remain very small around  
307 the average values. The curves for a SNR of 60 dB are not shown here as  
308 they are very similar to the one for a SNR of 30 dB but with lower standard  
309 deviations. We can thus conclude from that simulation that the damage in-  
310 dex  $DI_2$  is here also able to detect and to quantify the amount of damage in  
311 the nonlinear system with a high robustness to noise.

## 312 5. Experimental results

### 313 5.1. Plate specimens

314 The two composite plates employed in this study consist of a piece of  
315 aircraft composite fuselage. The dimensions of these structures are ( $400 \times$   
316  $300 \times 2 \text{ mm}^3$ ). They are both made up of 16 layers Carbone epoxy material.  
317 The layer sequences are: ( $0^\circ, 45^\circ, -45^\circ, 90^\circ, 90^\circ, -45^\circ, 45^\circ, 0^\circ$ ). An optimal  
318 placement of ten PZ29 piezoceramic patches with dimensions ( $30 \times 20 \times$   
319  $0.2 \text{ mm}^3$ ) has been achieved on these two structures using the controllability  
320 and observability gramians [21]. The composite plate shown in Fig. 6(a)  
321 was used as the baseline for damage detection. Fig. 6(b) shows the second  
322 composite plate, manufactured from the same material and layer sequences,  
323 having the same dimensions and PZT number and placement as the first one.  
324 However, in this plate, an calibrated impact damage with a 5 mm diameter  
325 was produced by projecting on the center of the plate a steel ball at a high  
326 and controlled velocity. This composite plate will be used as a damaged plate

327 example.

### 328 5.2. Data acquisition and Hammerstein Kernels estimation

329 The input excitation and the data acquisition were performed using a  
330 voltage amplifier (TREK MODEL 601C) and charge amplifiers (type 5011B).  
331 This excitation was applied sequentially to nine PZT elements and consists of  
332 an exponential sine sweep signal with  $f_1 = 100$  Hz,  $f_2 = 30$  kHz,  $T = 3.2588$  s  
333 and an amplitude of 10 V (see Sec. 2). Using a real time prototype system  
334 dSPACE, temporal signals were acquired with a sampling frequency  $f_s =$   
335 100 kHz from nine channels: one corresponding to the excitation applied to a  
336 given PZT actuator, and the eight others corresponding to the measurements  
337 collected by the PZT sensors. Under those conditions, the SNR is found to  
338 be approximately of 60 dB.

339 A first database has been built, by collecting 10 times in the healthy and  
340 damaged states the signals for all the paths starting from the PZT element  
341 number 7, located near the center of the plate, close to the damage. The  
342 aim of this database is to quantify the environmental variability existing  
343 for a given path by computing the damage index  $DI_1$  mean and standard  
344 deviation over the 10 trials and to infer a detection threshold for  $DI_2$  defined  
345 by Eq. (13). Another database has been built by collecting in each state  
346 (healthy or damaged) the signals for the  $9 \times 8 = 72$  paths existing between  
347 all pairs of PZT elements. The objective of this database is to illustrate the  
348 ability of both DIs to detect damages among the different paths and actuators  
349 that are considered. For both databases, the Hammerstein Kernels have been  
350 estimated using the method described in Sec. 2 up to an order of nonlinearity  
351  $N = 8$ . This choice has been done with respects to noise conditions and to

352 the length of the input exponential sine sweep [15].

### 353 *5.3. Sensibility to environmental noise and to damage for one actuator*

354 To assess the sensibility of the  $DI_1$  defined in Eq.(9) to the presence of  
355 environmental noise,  $DI_1$  values have been computed for all the repetitions  
356 for the healthy and damaged plates, as described in Sec. 5.2. In Fig. 7(a),  
357 the mean and standard deviation of the  $DI_1$  values computed over the 10  
358 repetitions for each path are shown for both states. From this figure, we can  
359 see that even in the healthy state, the  $DI_1$  values are around 0.77. This means  
360 that there is a non-negligible part of the energy in the nonlinear part of the  
361 output and thus that the system under study is nonlinear in its healthy state.  
362 This illustrates the fact that the proposed method can handle systems that  
363 are nonlinear in their healthy state. From that figure, it can also be seen that  
364 the variations caused by environmental noise on  $DI_1$  values remains relatively  
365 low and that the  $DI_1$  values for the damaged case are well above the  $DI_1$  values  
366 for the healthy state. As such, we can conclude that experimentally the  
367 proposed  $DI_1$  is not much sensitive to environmental noise and is effectively  
368 sensitive to the presence of the damage.

369 The damage index  $DI_2$  defined by Eq. (13) is comparing the nonlinear  
370 subspaces spanned by a reference state and by an unknown state. As so,  
371 this DI is relative by nature and a decision threshold needs to be defined in  
372 order to decide whether or not there is presence of a damage. To do so, we  
373 decided here to proceed experimentally by using the 10 repetitions for PZT  
374 7 in the healthy state. The first repetition has been chosen as the reference  
375 state, and the nine others as unknown (but healthy) states. The  $DI_2$  values  
376 obtained by comparing these unknown (but healthy) states to the reference

377 one are plotted on Fig. 7(b). It can be seen that the environmental noise  
378 does not cause large changes to these  $DI_2$  values. On the basis of these  
379 values, a decision threshold has then been defined as ten times the maximum  
380 value obtained previously. The factor ten is arbitrarily chosen but is thought  
381 here to be sufficiently large for reasonable decision making. This decision  
382 threshold is also plotted on Fig. 7(b). Now, the impact of environmental  
383 noise in the damaged case can be assessed by comparing, for each trial the  
384  $DI_2$  value obtained by comparing the healthy and damaged states. As shown  
385 in Fig. 7(b), for each trial, the obtained  $DI_2$  values are not so influenced by  
386 noise and are always above the decision threshold value. Thus, we can say  
387 that the  $DI_2$  defined by Eq. (13) is not very sensitive to noise and appears  
388 to be sensitive to the presence of the damage for this actuator.

#### 389 *5.4. Sensibility to the presence of the damage for all the actuators*

390 To assess the sensibility of the  $DI_1$  defined in Eq. (9) to the presence  
391 of the damage for different actuators and paths over the plate,  $DI_1$  values  
392 have been computed for each of the 72 paths measured on the healthy and  
393 damaged plates (as described in Sec. 5.2). For sake of brevity,  $DI_1$  values  
394 are presented here in a synthetic manner actuator by actuator. Fig. 8(a)  
395 depicts the mean and standard deviation of the  $DI_1$  values computed for all  
396 the paths starting from each of the nine PZT elements used as actuators for  
397 both the healthy and damaged states. From Fig. 8(a), it is clear that the  
398 damage introduced in the plate generates nonlinearities and that the  $DI_1$  as  
399 defined in Eq. (9) is sensitive to the presence of this damage. Indeed, for all  
400 the actuators, the mean  $DI_1$  values computed for all the paths starting from  
401 a given actuator are higher for the damaged state than for the healthy one.

402 To assess the sensibility of the  $DI_2$  defined in Eq. (13) to the presence  
403 of the damage for different actuators and paths over the plate,  $DI_2$  values  
404 have been computed for each of the 9 actuators using measurements from  
405 the healthy and damaged plates (as described in Sec. 5.2). These damage  
406 index values are compared in Fig. 8(b) to the detection threshold defined in  
407 the previous section. From Fig. 8(b), it is clear that the damage introduced  
408 in the plate generates nonlinearities and that the  $DI_2$  as defined in Eq. (13)  
409 is sensitive to the presence of this damage. Indeed, for all the actuators,  
410 the obtained  $DI_2$  values are higher for the damaged state than the chosen  
411 decision threshold.

## 412 6. Conclusion

413 In many cases, damages that appear on complex structures (such as  
414 cracks, impacts, or delaminations) can result in nonlinear dynamical re-  
415 sponses that may be used for damage detection. Furthermore, complex  
416 structures often exhibit a nonlinear behavior even in their healthy states.  
417 A robust and reliable SHM system must then be able to deal with nonlinear  
418 damages, and to distinguish between their effects and inherent nonlinearities  
419 in healthy structures. The first problem to be addressed is that the nonlinear  
420 models already in use are never general enough to encompass all the structure  
421 encountered in real life. The second problem is that the currently developed  
422 nonlinear models are not adequate for practical use of SHM systems. The  
423 work presented here attempts to face these two problems on the basis of a  
424 simple, but rather general, nonlinear model estimated by means of standard  
425 signal processing tools. This approach is based on the assumption that the



426 structure under study can be modeled as a cascade of Hammerstein models.  
427 The Exponential Sine Sweep Method, previously developed and validated  
428 by the authors for different purposes, is then used to estimate the different  
429 kernels of the model. Exponential sine sweeps are a class of sine sweeps that  
430 allow estimating a model in a wide frequency band from only one measure-  
431 ment. Two damage indexes are then build on the basis of this estimated  
432 model. The first one reflects the ratio of the energy contained in the non-  
433 linear part of the output versus the energy contained in its linear part and  
434 is specially suited for single-input single-output (SISO) systems. The second  
435 one is the angle between the subspaces described by the nonlinear parts of  
436 two set of outputs after a principal component analysis. This one is spe-  
437 cially suited for single-input multi-output (SIMO) systems. As a first step  
438 toward the use of this method for SHM, the sensitivity of the proposed DIs  
439 to the presence of damages as well as their robustness to noise are assessed  
440 numerically on SISO and SIMO systems and experimentally on two actual  
441 composite plates with surface-mounted PZT-elements (one healthy and one  
442 damaged).

443 The work presented here is however only a first step toward a larger use of  
444 this method in SHM. Indeed, it has be shown here that the proposed DIs are  
445 effectively sensitive to the presence of a non-linear damage and that they can  
446 potentially be helpful to quantify its extent. However, this approach can also  
447 be cast in the context of a statistical pattern recognition problem. Then, the  
448 DIs defined here, or other defined on the basis of the estimated model, can  
449 be used to train expert systems that are able to distinguish between different  
450 kind of damages [22].

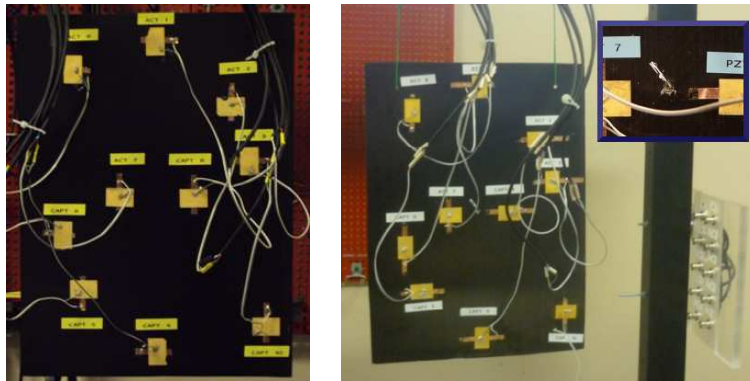
451 **References**

- 452 [1] C. R. Farrar, K. Worden, M. D. Todd, G. Park, J. Nichols, D. E. Adams,  
453 M. T. Bement, M. T. Farinholt, Nonlinear system identification for dam-  
454 age detection, Tech. rep., Los Alamos National Laboratory (2007).
- 455 [2] K. Worden, C. R. Farrar, J. Haywood, M. Todd, A review of nonlin-  
456 ear dynamics applications to structural health monitoring, *Structural*  
457 *Control & Health Monitoring* 15 (4) (2008) 540–567.
- 458 [3] J. M. Nichols, M. D. Todd, *Encyclopedia of Structural Health Monitor-*  
459 *ing*, John Wiley & Sons, Ltd, 2009, Ch. Nonlinear Features for SHM  
460 Applications.
- 461 [4] G. Kerschen, K. Worden, A. F. Vakakis, J. C. Golinval, Past, present  
462 and future of nonlinear system identification in structural dynamics,  
463 *Mechanical Systems and Signal Processing* 20 (3) (2006) 505–592.
- 464 [5] T. J. Johnson, D. E. Adams, Transmissibility as a differential indicator  
465 of structural damage, *Journal of Vibration and Acoustics-transactions*  
466 *of the Asme* 124 (4) (2002) 634–641.
- 467 [6] M. Haroon, D. E. Adams, Time and frequency domain nonlinear system  
468 characterization for mechanical fault identification, *Nonlinear Dynamics*  
469 50 (3) (2007) 387–408.
- 470 [7] Z. Q. Lang, Z. K. Peng, A novel approach for nonlinearity detection  
471 in vibrating systems, *Journal of Sound and Vibration* 314 (3-5) (2008)  
472 603–615.

- 473 [8] Z. Q. Lang, G. Park, C. R. Farrar, M. D. Todd, Z. Mao, L. Zhao,  
474 K. Worden, Transmissibility of non-linear output frequency response  
475 functions with application in detection and location of damage in mdof  
476 structural systems, *International Journal of Non-linear Mechanics* 46 (6)  
477 (2011) 841–853.
- 478 [9] D. E. Adams, C. R. Farrar, Application of frequency domain arx features  
479 for linear and nonlinear structural damage identification, *Smart Nonde-*  
480 *structive Evaluation For Health Monitoring of Structural and Biological*  
481 *Systems* 4702 (2002) 134–147.
- 482 [10] D. E. Adams, C. R. Farrar, Classifying linear and nonlinear structural  
483 damage using frequency domain arx models, *Structural Health Moni-*  
484 *toring - An International Journal* 1 (2) (2002) 185–201.
- 485 [11] L. Bornn, C. R. Farrar, G. Park, K. Farinholt, Structural health moni-  
486 toring with autoregressive support vector machines, *Journal of Vibration*  
487 *and Acoustics-transactions of the Asme* 131 (2) (2009) 021004.
- 488 [12] L. Bornn, C. R. Farrar, G. Park, Damage detection in initially nonlinear  
489 systems, *International Journal of Engineering Science* 48 (10) (2010)  
490 909–920.
- 491 [13] H. W. Chen, Modeling and identification of parallel nonlinear-systems -  
492 structural classification and parameter-estimation methods, *Proceedings*  
493 *of the IEEE* 83 (1) (1995) 39–66.
- 494 [14] A. Novak, L. Simon, F. Kadlec, P. Lotton, Nonlinear system identifica-

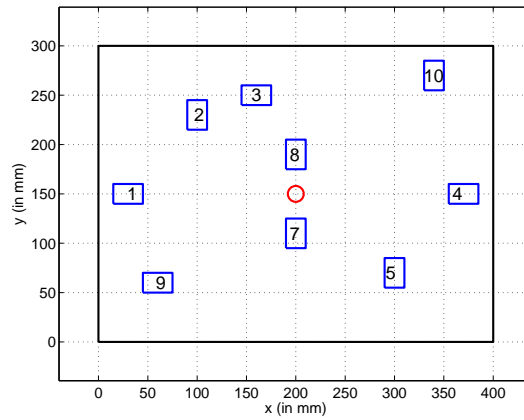
- 495 tion using exponential swept-sine signal, *Ieee Transactions On Instru-*  
496 *mentation and Measurement* 59 (8) (2010) 2220–2229.
- 497 [15] M. Rébillat, R. Hennequin, E. Corteel, B. F. G. Katz, Identification  
498 of cascade of hammerstein models for the description of nonlinearities  
499 in vibrating devices, *Journal of Sound and Vibration* 330 (5) (2011)  
500 1018–1038.
- 501 [16] G. Palm, Representation and approximation of non-linear systems .2.  
502 discrete-time, *Biological Cybernetics* 34 (1) (1979) 49–52.
- 503 [17] R. Hajrya, N. Mechbal, Principal component analysis and perturbation  
504 theory based robust damage detection of multifunctional aircraft struc-  
505 ture, *Structural Health Monitoring - An International Journal* 12 (3)  
506 (2013) 263–277.
- 507 [18] T. Jolliffe, I., *Principal Component Analysis* (second edition), Springer,  
508 1986.
- 509 [19] H. Golub, G., F. Van Loan, C., *Matrix Computation* (first edition),  
510 1983.
- 511 [20] C. Davis, W. Kahan, The rotation of eigenvectors by a perturbation. iii,  
512 *SIAM Journal on Numerical Analysis* 7 (1) (1970) 1–46.
- 513 [21] R. Hajrya, N. Mechbal, M. Verg, Active damage detection and local-  
514 ization applied to a composite structure using piezoceramic patches, in:  
515 *IEEE Conference on Control and Fault Tolerant Systems*, 2010.

- 516 [22] J. S. Uribe, N. Mechbal, M. Rébillat, K. Bouamama, M. Pengov, Prob-  
517 abilistic decision trees using SVM for multi-class classification, in: 2nd  
518 International Conference on Control and Fault-Tolerant Systems, 2013.



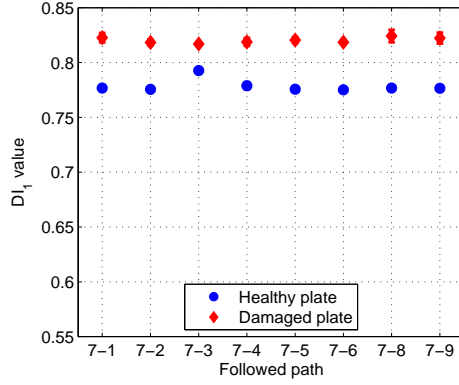
(a)

(b)

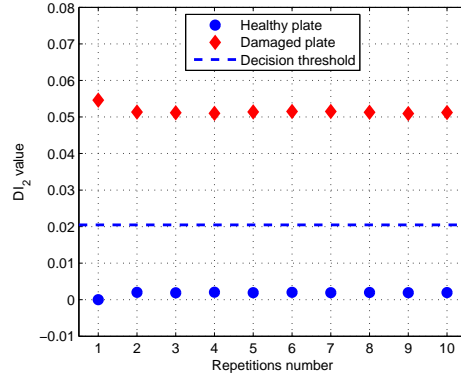


(c)

Figure 6: (a) Healthy and (b) damaged composite plates with a zoom on the impact damage. (c) Schematic representation of the plates under study (circle denotes damage position and rectangles stand for PZTs).

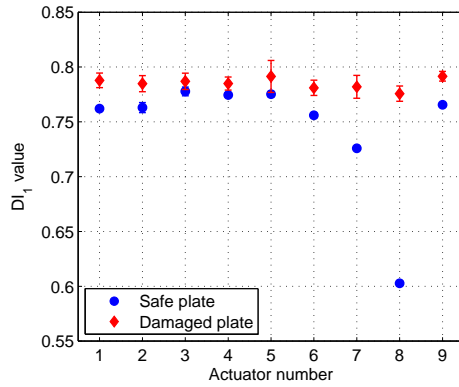


(a)

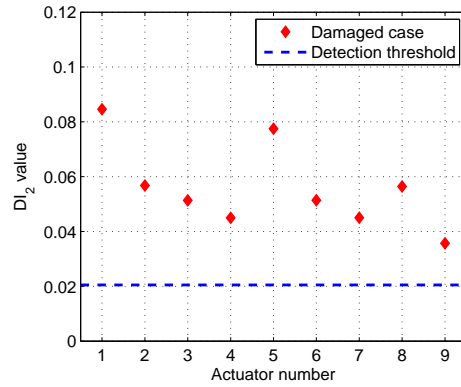


(b)

Figure 7: (a) Averages and standard deviations of  $DI_1$  values for the different paths starting from actuator 7. (b)  $DI_2$  values for the different repetitions for actuator 7 and definition of the detection threshold.



(a)



(b)

Figure 8: (a) Averages and standard deviations of  $DI_1$  values for the different actuators. (b)  $DI_2$  values for the different actuators in comparison to the detection threshold.